

Photophysical and Structural Properties of Saddle-Shaped Free Base Porphyrins: Evidence for an “Orthogonal” Dipole Moment

Igor V. Sazanovich,[†] Victor A. Galievsky,[†] Arie van Hoek,[‡] Tjeerd J. Schaafsma,[‡] Vladimir L. Malinovskii,[§] Dewey Holten,^{*,||} and Vladimir S. Chirvony^{*,†}

Institute of Molecular and Atomic Physics, National Academy of Sciences of Belarus, F. Skaryna Ave., 70, Minsk 220072, Belarus, Laboratory of Molecular Physics, Department of Biomolecular Sciences, Agricultural University, Dreijenlaan 3, 6703 HA Wageningen, The Netherlands, A.V. Bogatsky Physico-Chemical Institute, National Academy of Sciences of Ukraine, Lustdorfskaya doroga, 86, Odessa 270080, Ukraine, and Department of Chemistry, Washington University, St. Louis, Missouri 63130

Received: January 23, 2001; In Final Form: May 7, 2001

Ground- and excited-state absorption and fluorescence properties of three free base porphyrins with graded degrees of a macrocycle distortion have been studied. The different degrees of nonplanarity were introduced by successive addition of ethyl groups at the β -pyrrole positions of free base 5,10,15,20-tetraphenylporphyrin (H₂TPP): from four ethyl groups in *cis*-tetraethyl-TPP (H₂cTETPP) to six ethyl groups in hexaethyl-TPP (H₂HETPP) and eight ethyl groups in octaethyl-TPP (H₂OETPP). The static and dynamic optical properties of the compounds change systematically with an increase of the porphyrin macrocycle nonplanarity. These perturbations include significant broadening of the absorption and fluorescence bands, an increased spacing between the long-wavelength absorption and short-wavelength emission maxima, and reduced excited-state lifetimes. In nonpolar solvents, these perturbations directly reflect the steric/electronic consequences of the distortion of the porphyrin π -system. In polar media, all the photophysical consequences of nonplanar distortion are markedly enhanced as a function of solvent polarity. These effects derive from electronic interactions between the polar solvent molecules and the polar S₁(π, π^*) excited state of the nonplanar free base porphyrin. The origin of the polar nature of these nonplanar chromophores is indicated by semiempirical calculations, which show that free-base porphyrins with saddle-type macrocycle distortions have a permanent dipole moment (1–2 D) with a significant projection orthogonal to the nitrogen mean plane. Among the contributions to this macroscopic dipole moment are structural/electronic asymmetries derived from the pyrrole rings, N–H bonds and nitrogen lone pairs. The specific factors and the macroscopic dipole moment provide foci for solvent interactions that are amplified in nonplanar porphyrins relative to their planar counterparts. The studies demonstrate the strong interrelated effects of the conformation(s) involving the porphyrin macrocycle and its peripheral substituents, electronic structure, and solvent interactions (including macrocycle-nonplanarity-induced dipole moments) in dictating the photophysical properties of distorted porphyrins. The findings have implications for the function of tetrapyrrole cofactors in the biological proteins and for the use of nonplanar porphyrins in molecular optoelectronics.

Introduction

The three-dimensional structures of photosynthetic antenna systems and reaction centers, heme proteins, and related pigment–protein complexes routinely exhibit nonplanar distortions of the tetrapyrrole cofactors.¹ Synthetic porphyrins also exhibit significant and varied nonplanar distortions as a result of steric crowding of bulky or multiple peripheral substituents.^{2–4} These nonplanar synthetic compounds have substantially altered redox potentials, optical and Raman spectra, emission yields, and excited-state lifetimes relative to planar analogues.^{2–10} These combined findings have led to the suggestion that nonplanar distortions imposed by a protein matrix may tune functional

properties of the tetrapyrrole cofactors toward energy, electron, and ligand transport.¹⁰

Static protein-induced nonplanar distortions of tetrapyrrole cofactors may be complemented by dynamic structural distortions in the cofactor that in turn elicit effects in the protein during specific biological reactions. Such reciprocal tetrapyrrole \leftrightarrow protein interactions may be amplified by differences in the electron-density distributions (and thus polarity and polarizability) of the various accessible tetrapyrrole conformers. For example, if the domed intermediate formed by O₂ release by hemoglobin or myoglobin^{11a} develops a sufficiently large permanent dipole moment,^{11b} then this nonplanar and polar intermediate will elicit both electronic and structural responses in the protein matrix. Similar cofactor \leftrightarrow protein structural/electronic responses may be operable in porphyrin-based redox and catalytic proteins.

Stronger underpinnings for such possibilities have emerged from recent studies on synthetic nonplanar porphyrins. Photophysical studies on Ni(II) 5,10,15,20-tetra-*tert*-butylporphyrin (NiT(*t*-Bu)P) have revealed that nonplanar macrocycle distortions can give rise to a polar excited state of the molecule. This

* To whom correspondence should be addressed. E-mail: chirvony@imaph.bas-net.by or holten@wuchem.wustl.edu.

[†] Institute of Molecular and Atomic Physics, National Academy of Sciences of Belarus.

[‡] Laboratory of Molecular Physics, Department of Biomolecular Sciences, Agricultural University, The Netherlands.

[§] A.V. Bogatsky Physico-Chemical Institute, National Academy of Sciences of Ukraine.

^{||} Department of Chemistry, Washington University.

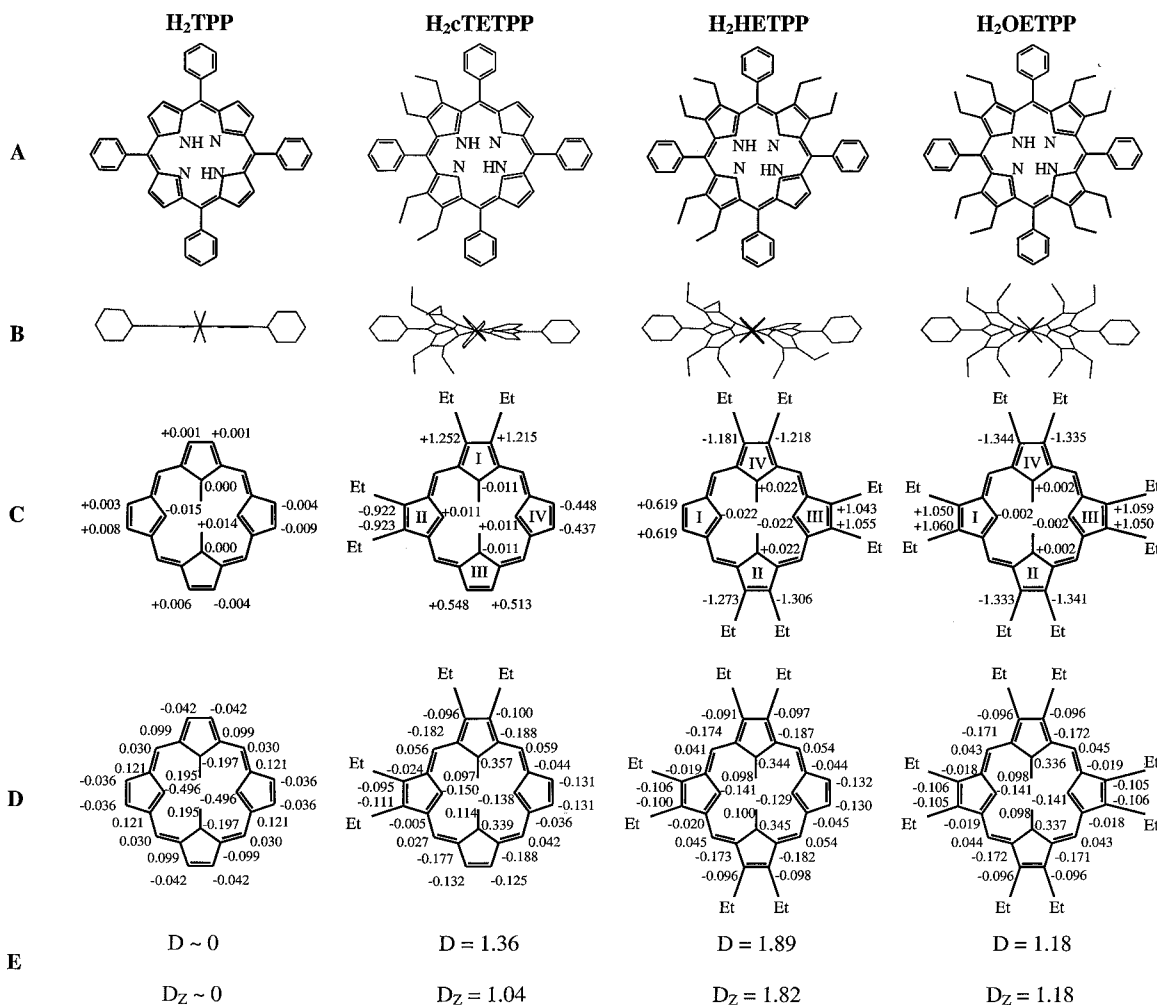


Figure 1. Molecular details for planar H_2TPP and the three nonplanar porphyrins with increasing degrees of distortion in the order $H_2cTETPP < H_2HETPP < H_2OETPP$. For each compound, shown are (A) chemical composition, (B) side-views of the calculated energy-minimized structure, (C) calculated deviations from the mean plane of the four nitrogens (for the three nonplanar porphyrins, the numbering of the quadrants referred to in Table 5 is shown within pyrrole rings), (D) calculated charge-densities, and (E) calculated permanent dipole moment and its Z -axis (orthogonal to the mean nitrogen plane) projection in Debyes.

photoexcited form has significant interactions with its environment that have pronounced consequences on the properties of the chromophore. In particular, the lifetime of the (d,d) excited state of $NiT(t-Bu)P$ is found to change by over 6 orders of magnitude (picoseconds to microseconds) with solvent dielectric properties and temperature.^{8b} In contrast, the (d,d)-state lifetimes of nominally planar analogues such as nickel(II) 5,10,15,20-tetraphenylporphyrin ($NiTPP$) vary only about 4-fold (100–400 ps) under the same variation in environmental conditions. Although quite provocative, directly translating the conclusions on nonplanar nickel porphyrins such as $NiT(t-Bu)P$ to other porphyrins requires several caveats. One is that the inferred excited-state dipole moment may be induced to a large degree by the photoinduced change in the d-orbital electronic configuration of the metal. Second, the metal excited state may not only cause changes in the macrocycle planarity (due to electron–electron repulsion), but also involve charge transfer between metal- d and macrocycle- π orbitals which itself causes electronic asymmetry. Additionally, the nonluminescent behavior of the nickel porphyrins limits the applicable static and time-resolved optical techniques for exploring the interrelated effects of macrocycle distortions and dielectric properties.

Recent studies have shown that, even in the absence of a central metal, nonplanar free-base porphyrins or their diacid derivatives display significantly perturbed photophysical proper-

ties compared to planar counterparts.^{4–9} What is not clear is the extent to which the dielectric properties of these macrocycles are affected by nonplanarity because they lack the d-orbital effects of a central metal on the π -system of the macrocycle. Additionally, free base porphyrins have lower symmetry than metalloporphyrins due to the presence of hydrogens on only two of the four central nitrogens. Thus, the question arises as to whether this latter effect when combined with nonplanar distortions (even if symmetric) may give rise to a static dipole moment (and associated local structural/electronic asymmetries) before and/or after photoexcitation. To address these issues, we have studied the ground- and excited-state properties of three free base porphyrins with graded degrees of a macrocycle distortion. The different degrees of nonplanarity were introduced by successive addition of ethyl groups at the β -pyrrole positions of the parent free base 5,10,15,20-tetraphenylporphyrin (H_2TPP) macrocycle, as indicated by X-ray crystallography.³ The molecules, depicted in Figure 1 (row A), are 2,3,7,8-tetraethyl-5,10,15,20-tetraphenylporphyrin ($H_2cTETPP$), 2,3,7,8,12,13-hexaethyl-5,10,15,20-tetraphenylporphyrin (H_2HETPP) and 2,3,7,8,12,13,17,18-octaethyl-5,10,15,20-tetraphenylporphyrin (H_2OETPP).

The photophysical properties of these complexes were examined using static and time-resolved optical techniques. Trends in macrocycle distortion and permanent dipole moments

(and associated local/specific structural/electronic factors), were probed using quantum chemical calculations. The studies have enabled us to find qualitative correlations between (1) the nature and degree of macrocycle distortions, (2) the calculated static dipole moments, which have marked components orthogonal to the porphyrin nitrogen mean plane, and (3) the highly solvent and temperature dependent spectral and excited-state relaxation properties that are observed. The studies reinforce the extremely close connections between porphyrin conformation (involving the macrocycle and its peripheral substituents), electronic characteristics, and solvent interactions in nonplanar porphyrins. The results also specifically demonstrate the importance of macroscopic/local electronic asymmetries, including macrocycle-nonplanarity-induced dipole moments, in dictating the electronic properties and excited-state deactivation mechanisms of nonplanar tetrapyrroles.

Experimental Section

The compounds H₂cTETPP, H₂HETPP, H₂OETPP, and H₂-TPP were synthesized and purified following the published methods.^{3,12} Absorption spectra were recorded using a Cary 500 Scan spectrophotometer. Corrected steady-state fluorescence and fluorescence excitation spectra were recorded on SDL-2 fluorescence spectrometer (LOMO production, Russia) that measures emission spectra up to 1100 nm. Steady-state fluorescence measurements employed a 90° angle between the excitation and the detection paths.

Time-resolved fluorescence measurements were carried out using a time-correlated photon counting setup as described earlier.¹³ The pulse duration of excitation pulses was ~4 ps full width at half-maximum (fwhm), the maximum pulse energy was ~100 pJ, and the excitation wavelength could be tuned over the whole visible and near UV regions. Samples for the fluorescence kinetics measurements were in 1.0 cm³, 1 cm light path fused silica cuvettes. The emission was selected via a polarizer set at the magic angle (54.7°). The fluorescence was collected at an angle of 90° with respect to the direction of the excitation beam and passed through a monochromator. Detection electronics were standard time correlated single photon counting modules with some improvements.¹⁴ The instrument response function was ~35 ps fwhm. For obtaining a dynamic instrumental response as a reference for deconvolution,¹⁵ a reference light-scattering sample was used. Data analysis was performed on a PC computer with use of a homemade software.

All measurements in this work were carried out in solutions containing dissolved oxygen of air. (Note that the air-equilibrated dissolved oxygen should not decrease the corresponding fluorescence lifetimes from the actual values by more than ~10% because H₂cTETPP, H₂HETPP, and H₂OETPP exhibit fluorescence lifetimes of only a few nanoseconds.) When necessary, triethylamine was added to the samples to deprotonate any porphyrin dications to the neutral species. (All measurements were in fact carried out both in the presence and absence of triethylamine; the same results were generally obtained, with the exception of some protonation after extended periods, in the absence of the amine.) The porphyrin concentrations were (1–5) × 10⁻⁶ M. For the measurements at 77 K, the mixtures used were tetrahydrofuran/diethyl ether (1:1) and, when triethylamine was added, toluene/diethyl ether (1:3). These mixtures provide good solubility of the porphyrins as well as good transparent low-temperature glasses.

Geometry optimizations were performed using the semiempirical PM3 method¹⁶ in the framework of the HyperChem program¹⁷ to obtain optimized geometries of the molecules of

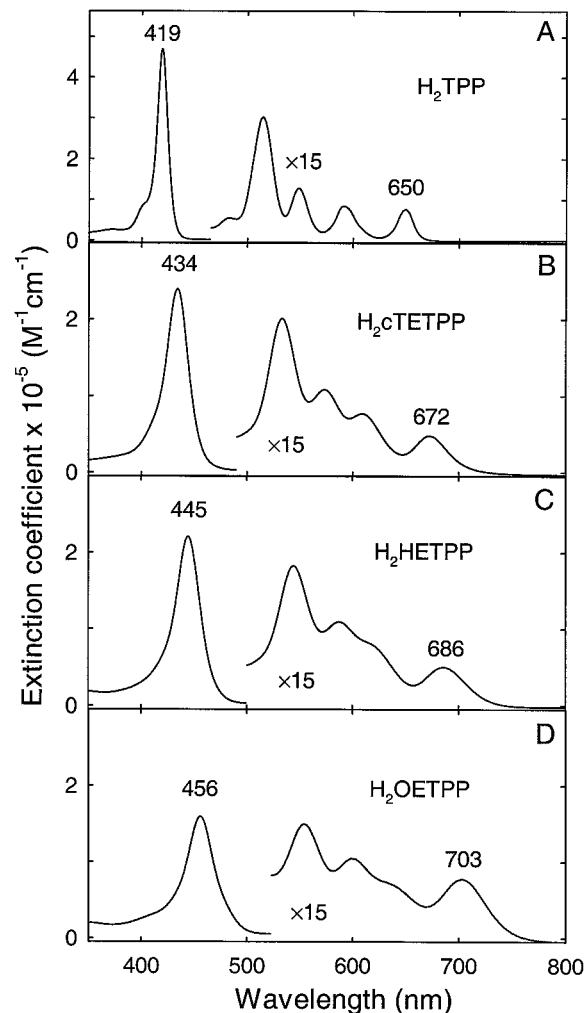


Figure 2. Room-temperature ground-state absorption spectra of H₂cTETPP (B), H₂HETPP (C) and H₂OETPP (D) (all in methylene chloride) in comparison with that of H₂TPP (A, in benzene). The Q-bands have been multiplied by a factor of 15 for clarity. Peak wavelengths (in nm) are indicated.

H₂TPP, H₂cTETPP, H₂HETPP, and H₂OETPP as input for calculations of their excited and ground states properties. Both the ZINDO/S¹⁸ and the PM3 methods were used to calculate the wavelengths and oscillator strengths of the S₀ → S_n electronic transitions, dipole moments in the ground and excited states, and their electronic charge distribution. The configuration–interaction calculations included single excitations from the 10 top-filled orbitals to the 10 lowest-empty orbitals. Note that conclusions from these calculations were based on the trends for the compounds and not from absolute values of the quantities.

Results

Ground-State Absorption Spectra. Figure 2 shows room-temperature electronic absorption spectra of all the three nonplanar porphyrins relative to the planar “unsubstituted” reference compound H₂TPP. The spectral data in solvents of differing polarity and at different temperatures are summarized in Table 1. Compared to H₂TPP, the strong near-UV Soret band of H₂cTETPP has about one-half the peak extinction coefficient, is about twice as wide, and is red shifted by about 15 nm (to 434 nm in toluene). Similarly, the series of four Q-bands are broader and have reduced peak intensity for H₂cTETPP compared to H₂TPP (leading to less structure in the manifold),

TABLE 1: Summary of Spectral Data

solvent	E_T^N ^a	H ₂ TETPP					H ₂ cTETPP				
		B ^b (nm)	$\Delta\nu_B^c$ (cm ⁻¹)	Q ₃₀₀ (ab) ^d (nm)	Q ₃₀₀ (fl) ^e (nm)	Δ (ab/fl) ^f (cm ⁻¹)	B ^b (nm)	$\Delta\nu_B^c$ (cm ⁻¹)	Q ₃₀₀ (ab) ^d (nm)	Q ₃₀₀ (fl) ^e (nm)	Δ (ab/fl) ^f (cm ⁻¹)
<i>n</i> -hexane	0.009	415	700	651	652	<50	429	1450	675	696	450
toluene	0.099	419	700	650	656	150	434	1400	675	699	500
acetone	0.355	414	700	646	650	100	429	1450	672	697	550
acetonitrile	0.460	414	700	645	650	100	429	1500	672	702	650
at 77K ^g		419	500	645	647	50	435	800	668	673	100
solvent	E_T^N ^a	H ₂ HETPP					H ₂ OETPP				
		B ^b (nm)	$\Delta\nu_B^c$ (cm ⁻¹)	Q ₃₀₀ (ab) ^d (nm)	Q ₃₀₀ (fl) ^e (nm)	Δ (ab/fl) ^f (cm ⁻¹)	B ^b (nm)	$\Delta\nu_B^c$ (cm ⁻¹)	Q ₃₀₀ (ab) ^d (nm)	Q ₃₀₀ (fl) ^e (nm)	Δ (ab/fl) ^f (cm ⁻¹)
<i>n</i> -hexane	0.009	441	1500	690	720	600	453	1700	705	746	800
toluene	0.099	443	1450	687	723	700	455	1650	706	750	850
acetone	0.355	439	1550	685	730	900	452	1900	707	768	1100
acetonitrile	0.460	440	1650	684	750	1300	453	2000	710	778	1250
at 77K ^g		439	900	669	681	250	460	1200	707	723	300

^a Normalized empirical parameter of solvent polarity.^{19b} ^b Position of the Soret band (± 1 nm). ^c Full width at half-maximum of the Soret band (± 50 cm⁻¹). ^d Position of the Q₃₀₀ band maximum in absorption (± 1 nm). ^e Position of the Q₃₀₀ band maximum in fluorescence (± 1 nm). ^f Shift between the Q₃₀₀(ab) maximum and Q₃₀₀(fl) maximum (± 50 cm⁻¹). ^g The data were obtained in solvent mixture toluene/diethyl ether (1:3) or tetrahydrofuran/diethyl ether (1:1).

with the Q_X(0,0)-band maximum red shifted by about 20 nm (to 675 nm in toluene). This pattern of a less intense, broader, and red shifted Soret band and reduced Q-region structure continues as the number of peripheral ethyl substituents increases in going from H₂cTETPP to H₂HETPP and to H₂OETPP. Two other points are noteworthy: (1) the relative (to the other Q-bands) intensity of the Q_X(0,0) band increases along this series (Figure 2), and (2) the spectra do not change markedly among the solvents used, except for broadening in the more polar media (Table 1).

Fluorescence Spectra. The corresponding emission spectra of the three compounds in different solvents are shown in Figure 3 and summarized in Table 1. Even in nonpolar solvents such as *n*-hexane and toluene, increasing the number of peripheral β -ethyl substituents results in systematic red shift of the fluorescence spectra as well as less structure and reduced resolution of the Q_X(0,1) band from the Q_X(0,0) transition. This shift of the Q_X(0,0) fluorescence maximum among the compounds is larger than the corresponding shift of the Q_X(0,0) absorption band. The result is that the spacing between the long-wavelength absorption and the short-wavelength fluorescence maxima, denoted Δ (ab/fl), increases from 500 to 850 cm⁻¹ (in toluene) in going from H₂cTETPP to H₂OETPP (Table 1). The absorption/fluorescence spacings for all three compounds is significantly larger than that for H₂TETPP, which has Δ (ab/fl) \sim 150 cm⁻¹ in toluene.

For each compound, an increase in the solvent polarity¹⁹ results in an increase in the long-wavelength shift of the fluorescence spectrum and a corresponding increase of the Δ (ab/fl) value. This tendency is the least pronounced for H₂cTETPP (Δ (ab/fl) = 650 cm⁻¹ in acetonitrile vs 450 cm⁻¹ in *n*-hexane) than for H₂HETPP (1300 vs 600 cm⁻¹) and for H₂OETPP (1250 vs 800 cm⁻¹). Additionally, an increase of the solvent polarity for each compound results in decreasing fluorescence structure, leading to a featureless bell-shaped spectrum (Figure 3).

Figure 4 shows fluorescence spectra of all the three compounds obtained in toluene/diethyl ether (1:3) mixture at 296 and 77 K. In contrast to the broader and less featured room-temperature spectra, the emission of all the three compounds at 77 K consists of two fairly well resolved Q_X(0,0) and Q_X(0,1) bands that are markedly blue shifted from the 296-K

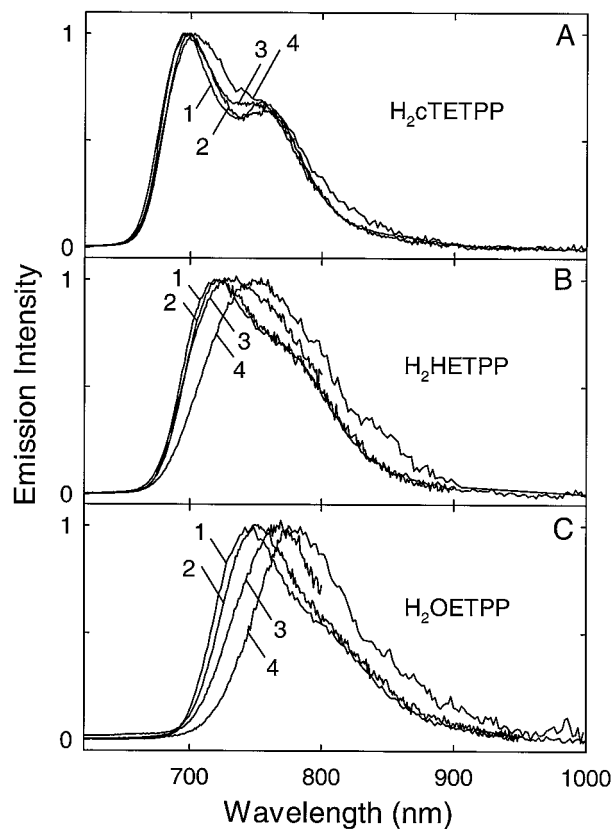


Figure 3. Normalized fluorescence spectra of H₂cTETPP (A), H₂HETPP (B) and H₂OETPP (C) in different solvents at 293 K obtained by excitation into the Soret band. Labels near the curves mark spectra obtained in *n*-hexane (1), toluene (2), acetone (3) and acetonitrile (4).

positions. Given that the absorption spectra are not altered as significantly with temperature, the Δ (ab/fl) spacings are much smaller at 77 vs 296 K (100 vs 450–650 cm⁻¹ for H₂cTETPP, 250 vs 600–1300 cm⁻¹ for H₂HETPP, and 300 vs 800–1250 cm⁻¹ for H₂OETPP; Table 1). Additionally, all three compounds at 77 K exhibit a dependence of their fluorescence positions on the excitation wavelength and of their fluorescence excitation spectra on the detection wavelength. This effect is the most pronounced for H₂HETPP (Figure 5) and H₂OETPP (not

TABLE 2: Fluorescence Decay Parameters in Different Solvents at Room Temperature^a

solvent	E_T^N ^b	$H_2cTETPP$		H_2HETPP		H_2OETPP	
		τ_1 (ns)	τ_2 (ns)	τ_1 (ns)	τ_2 (ns)	τ_1 (ns)	τ_2 (ns)
<i>n</i> -hexane	0.009	0.72 (0.08)	3.02 (0.92)	0.67 (0.10)	1.64 (0.90)	0.43 (0.16)	1.02 (0.84)
toluene	0.099	0.95 (0.08)	2.76 (0.92)	0.67 (0.13)	1.47 (0.87)	0.39 (0.18)	0.91 (0.82)
acetonitrile	0.460	0.64 (0.18)	1.59 (0.82)	0.40 (0.71)	0.90 (0.29)	0.15 (0.32)	0.68 (0.68)

^a The two longest-lived fluorescence lifetimes (time constants) from the triexponential fitting of the emission decay profiles. Standard errors ± 0.05 ns. The values in parentheses are the relative amplitudes of the decay components. The measurements were carried out using 440 nm excitation and detection at 680 nm for $H_2cTETPP$, 695 nm for H_2HETPP , and 720 nm for H_2OETPP . ^b Normalized empirical parameter of solvent polarity.^{19b}

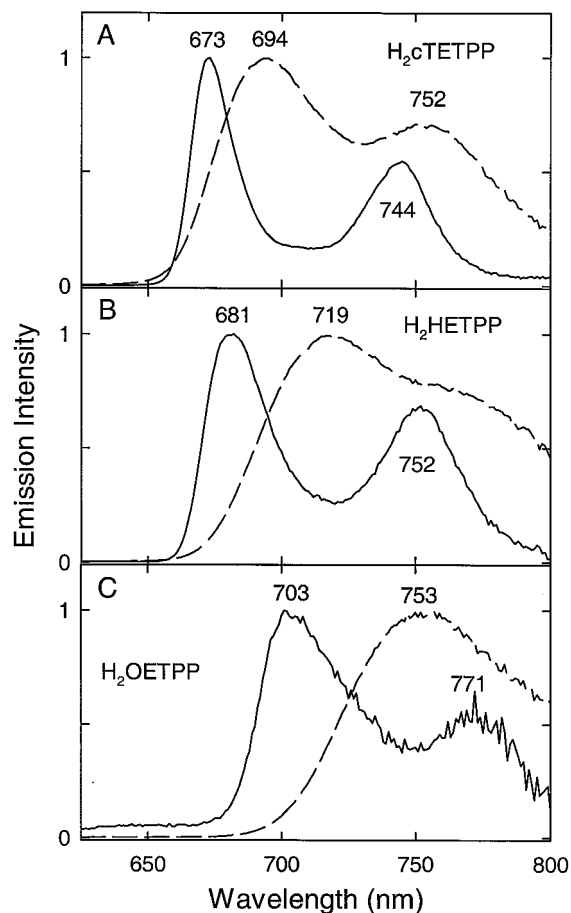


Figure 4. Normalized fluorescence spectra of $H_2cTETPP$ (A), H_2HETPP (B), and H_2OETPP (C) in the solvent mixture toluene/diethyl ether (1:3) at 77 K (solid line) and at 293 K (dashed line) obtained by excitation into the Soret bands. Numbers near peaks are wavelengths (in nm) of the corresponding fluorescence maxima.

shown). Such a dependence on excitation and detection wavelength is not found at 296 K.

Several additional points regarding these temperature-dependent effects are noteworthy. Similar results at 77 K to those described above for THF/diethyl ether (1:1) were obtained in toluene/diethyl ether (1:3). At room temperature, the emission (and absorption) properties in these two solvent mixtures differed from one another according to mean solvent polarity of the mixture, in a manner consistent with the findings in pure solvents. Thus, specific effects of the solvents such as hydrogen bonding involving THF that may contribute to the photophysical properties are of lesser importance than other factors such as solvent polarity.

Fluorescence Kinetics. The fluorescence time profiles were measured for the three compounds in three solvents of different polarity at room temperature (Figure 6 and Table 2) Adequate

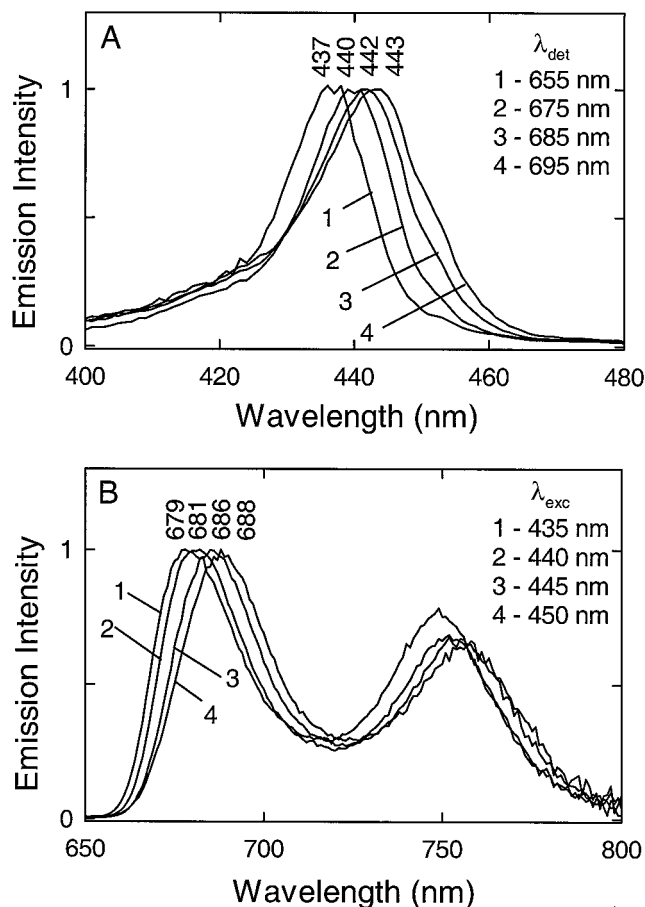


Figure 5. Dependencies of the fluorescence excitation (A, Soret band region) and fluorescence (B) spectra of H_2HETPP in the solvent mixture toluene/diethyl ether (1:3) at 77 K on the registration and excitation wavelengths, respectively. Numbers near peaks are wavelengths (in nm) of the corresponding maxima.

fits to the fluorescence kinetics for each compound requires a triexponential function of the form $I(t) = A_0 \cdot \exp(-t/\tau_0) + A_1 \cdot \exp(-t/\tau_1) + A_2 \cdot \exp(-t/\tau_2)$. The second and third terms describe deactivation of the excited $S_1(\pi, \pi^*)$ state; the first term, which has time constant $\tau_0 \leq 10$ ps (near the instrument time resolution) and will be not discussed here, corresponds to ultrafast relaxation processes in the excited $S_1(\pi, \pi^*)$ state.²⁰ The long-lived component τ_2 dominates the decay and generally comprises about 80–90% of the amplitude (Table 2). The time constants of both decay components for each solvent decrease with increasing number of β ethyl substituents on the macrocycle (e.g., in *n*-hexane, τ_2 decreases from 3.02 ns for $H_2cTETPP$ to 1.02 ns for H_2OETPP , and τ_1 decreases from 0.72 to 0.43 ns). For each compound, the fluorescence lifetimes generally decrease about 2-fold overall with increasing solvent polarity in going from *n*-hexane to toluene and to acetonitrile.

TABLE 3: Temperature Dependence of the Fluorescence Decay Parameters^a

temp K	H ₂ cTETPP		H ₂ HETPP		H ₂ OETPP	
	τ_1 (ns)	τ_2 (ns)	τ_1 (ns)	τ_2 (ns)	τ_1 (ns)	τ_2 (ns)
276	0.94 (0.07)	3.14 (0.93)	0.72 (0.09)	1.72 (0.91)	0.37 (0.26)	0.96 (0.74)
300	0.95 (0.08)	2.76 (0.92)	0.67 (0.13)	1.47 (0.87)	0.39 (0.18)	0.91 (0.82)
343	0.85 (0.15)	1.80 (0.85)	0.64 (0.56)	1.14 (0.44)	0.36 (0.17)	0.75 (0.83)

^a Fluorescence lifetimes (time constants of the biexponential fitting of the fluorescence decay); the numbers in parentheses are relative amplitudes of the two decay components. Standard errors ± 0.05 ns. The kinetic measurements were carried out at 680 nm for H₂cTETPP, at 695 nm for H₂HETPP, at 720 nm for H₂OETPP. The excitation was at 440 nm in all cases. Toluene was used as a solvent.

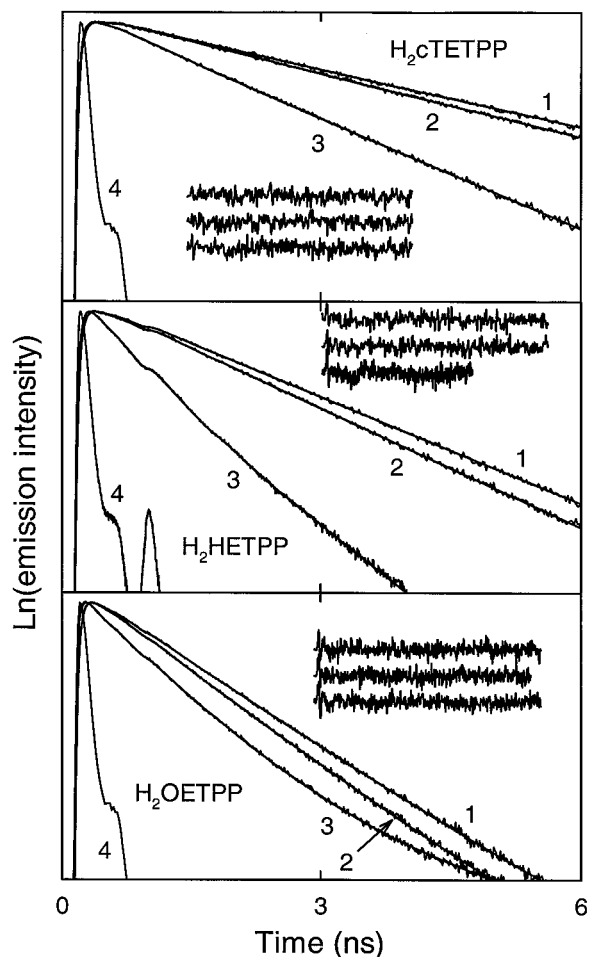


Figure 6. Fluorescence decay kinetics of H₂cTETPP, H₂HETPP and H₂OETPP in different solvents at 300 K (in semilogarithmic scale). Labels near the curves mark kinetics obtained in *n*-hexane (1), toluene (2) and acetonitrile (3) and the instrument response (4). Experimental kinetics are shown together with the respective calculated triple-exponential fitting curves. Residuals in inserts correspond to the kinetics 1 (top), 2 (middle), and 3 (bottom). The fluorescence detection wavelengths are near maxima of the corresponding fluorescence spectra. The excitation was at 440 nm in all cases.

The fluorescence decay for each compound lengthens markedly with a decrease in temperature, with the effect residing largely in the dominant, long-lived τ_2 component (Figure 7 and Table 3). For example, τ_2 for H₂cTETPP (in toluene) is 3.14 ns at 276 K, 2.76 ns at 300 K, and 1.80 ns at 343 K. The effect of temperature becomes less pronounced as the number of β -ethyl groups increases and the τ_2 value simultaneously decreases (e.g., τ_2 changes by about 40% between 276 and 343 K for H₂cTETPP but by 20% for H₂OETPP). Activation enthalpies of 1.6 kcal/mol (550 cm⁻¹) for H₂cTETPP, 1.2 kcal/mol (430 cm⁻¹) for H₂HETPP, and 0.6 kcal/mol (220 cm⁻¹) for H₂OETPP were estimated from the 276–343-K data in toluene for the dominant

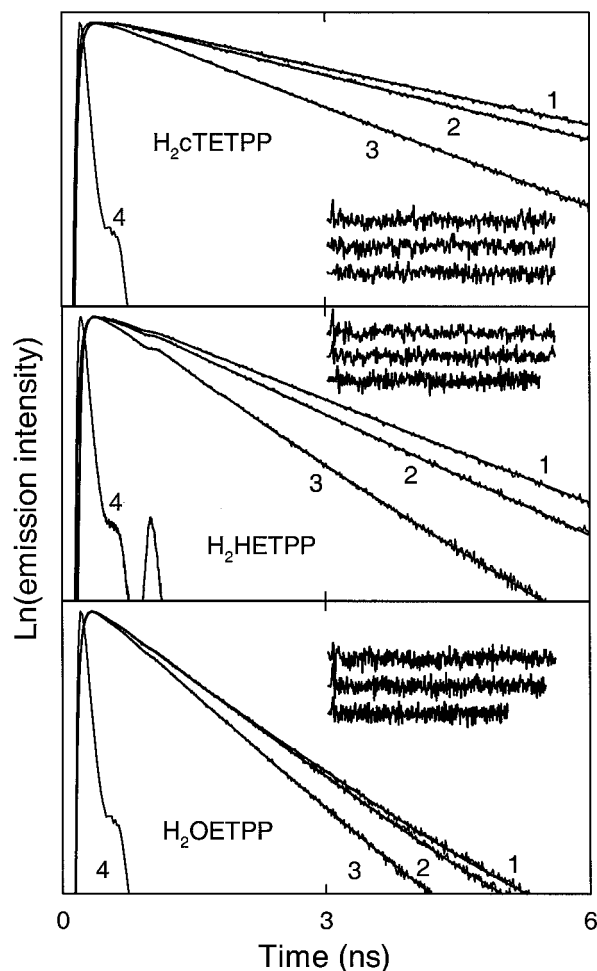


Figure 7. Fluorescence decay kinetics of H₂cTETPP, H₂HETPP and H₂OETPP at different temperatures in toluene (in semilogarithmic scale). Numbers near curves indicate kinetics obtained in at 276 K (1), 300 K (2), and 343 K (3) and the instrument response (4). Experimental kinetics are shown together with the respective calculated triple-exponential fitting curves. Residuals in inserts correspond to the kinetics 1 (top), 2 (middle), and 3 (bottom). The fluorescence detection wavelengths are near maxima of the corresponding fluorescence spectra. The excitation was at 440 nm in all cases.

long-lived τ_2 component assuming Arrhenius behavior. The corresponding results in acetonitrile show that both the activation enthalpies and frequency factors depend on solvent polarity (Table 4). Preliminary measurements at 77 K indicate that the τ_2 values (4.05 ns ($A_2 = 0.80$) for H₂cTETPP, 2.63 ns (0.70) for H₂HETPP, and 1.50 ns (0.60) for H₂OETPP) are about 1.5-fold larger than those in *n*-hexane at 296 K, whereas the τ_1 values are approximately the same.

Semiempirical Calculations. Optimized structures were calculated for each of the three ethyl-substituted compounds using semiempirical PM3 calculations. Side views of the

TABLE 4: Arrhenius Parameters from the Temperature-Dependent Fluorescence Decays^a

solvent	H ₂ cTETPP		H ₂ HETPP		H ₂ OETPP	
	ΔE (cm ⁻¹)	k_0 (10 ⁹ s ⁻¹)	ΔE (cm ⁻¹)	k_0 (10 ⁹ s ⁻¹)	ΔE (cm ⁻¹)	k_0 (10 ⁹ s ⁻¹)
toluene	550	5	430	5	220	3
acetonitrile	840	37	350	6	350	8

^a Activation enthalpies (ΔE) and frequency factors (k_0) derived from the temperature dependencies of the long-lived components of the fluorescence decay kinetics assuming Arrhenius-type behavior.

optimized structures showing deviations from the mean plane are shown in Figure 1 (row B). This figure also shows deviations from the mean plane of the four nitrogens (row C). These structures, described further below, are generally in good agreement with the available X-ray data³ (in terms of the relative magnitudes of the deviations and their asymmetries) and were used as input for calculation of other electronic properties. In this regard, Table 5 compares the average deviations of the two C_b positions of each porphyrin pyrrole from the least-squares plane of four nitrogen atoms (ΔC_b) calculated here and determined from the X-ray data.³ This comparison is particularly relevant because for saddle-type distortions the largest deviations from planarity are observed for C_b carbons.

The positions of the S₀ → S_n (π, π^*) electronic transitions and their oscillator strengths were calculated by the PM3 and ZINDO/S methods for the three optimized structures. The results of these calculations are in good qualitative agreement with the absorption measurements. In particular, the calculations predict a red shift of the Q and Soret optical transitions in going from the less distorted H₂cTETPP to the more distorted H₂HETPP and especially for the more distorted H₂OETPP (not shown). However, the most interesting result of these calculations is the prediction of a rather large static dipole moment (1–2 D) for each compound, in both the ground and the lowest excited singlet states. The ZINDO/S and PM3 methods gave qualitatively similar results, and we report here only the latter values for the ground state (Figure 1, row E). These dipole moments incorporate both the structures of the molecules, most notably the deviations of the macrocycle atoms from the mean nitrogen plane (Figure 1, row C), as well as the calculated charge-density distributions (Figure 1, row D). Specific local structural/electronic asymmetries contributing to the macroscopic dipole moments (and potentially to the photophysical properties) will be given in the Discussion section.

The calculations predict a dipole moment of 1.36 D for H₂cTETPP, 1.89 D for H₂HETPP, and 1.18 D for H₂OETPP. For the latter two compounds, this static dipole moment is essentially normal to the plane formed by the four pyrrole nitrogens; in particular, the Z-component of the dipole moment (D_z) is approximately the same as the total dipole (Figure 1). In the case of H₂cTETPP, the D_z projection is somewhat less than

the total (1.04 vs 1.36 D), which corresponds to a dipole direction of about 50° with respect to the mean nitrogen plane. The reference compound H₂TPP showed practically a complete absence of any static dipole moment.

We carried out two additional calculations to probe whether the dipole moments (and photophysical properties) in the highly substituted free base porphyrins derive from a true effect of macrocycle nonplanarity or from a combined electronic response to the differing electronic characteristics of the ethyl and phenyl substituents.²¹ First, a calculation was performed on a near-planar H₂OETPP structure. Although the lowest-energy structure of this molecule is saddle-shaped, a near-planar local minimum can be generated by replacing the eight β -pyrrole hydrogens of H₂TPP by ethyl groups, followed by the full geometry optimization. PM3 calculations based on this near-planar H₂OETPP structure reveal a dipole moment ~ 0.06 D, which is only $\sim 5\%$ of that for the saddle structure. In the second calculation, the eight ethyl substituents of the optimized saddle structure of H₂OETPP were replaced by hydrogens without further structure optimization. Calculations based on this structure gave a dipole moment having essentially the same magnitude and direction as for the highly nonplanar saddle structure of this molecule.

Discussion

General Considerations. Crystallographic studies show that H₂cTETPP, H₂HETPP, and H₂OETPP are nonplanar and that the overall extent of the out-of-plane distortion increases successively with the number of β -ethyl substituents.³ The same characteristics are seen in the optimized structures shown in Figure 1. The most distorted of these compounds is H₂OETPP. This compound has all eight β -pyrrole positions substituted and adopts a symmetric saddle structure. Analogous “saddle-type” distortions are seen for the three ethyl-substituted pyrrole rings of H₂HETPP and the two adjacent, ethyl-substituted pyrrole rings of H₂cTETPP. As a result of these substituent patterns, the latter two molecules have asymmetric structures as well as reduced overall degrees of distortion relative to H₂OETPP. For saddle-type distortions, the largest deviations from planarity are observed for C_b carbons (to which the ethyl groups are attached). Thus, it is reasonable to consider an average deviation of the eight C_b positions from the least-squares plane of four nitrogen atoms^{1c} (ΔC_b) as a measure of the overall degree of nonplanarity. The crystallographic data reveals ΔC_b values of 0.76, 0.95, and 1.17 Å for H₂cTETPP, H₂HETPP, and H₂OETPP, respectively, as compared to the value of 0.06 Å for H₂TPP.³ The same trend is obtained from the minimized structures calculated here (see row C in Figure 1 and Table 5).

The static and dynamic photophysical properties that we have found for these compounds track well with the increase in nonplanarity in the order H₂cTETPP < H₂HETPP < H₂OETPP. This correlation (which is not linear) is manifested in the

TABLE 5: Average Deviations of the C_b Carbons from the Mean Nitrogen Plane (ΔC_b)^a

compound	data source ^b	four-quadrant				
		average	quadrant I	quadrant II	quadrant III	quadrant IV
H ₂ cTETPP	calculated	0.78	1.24	-0.92	0.53	-0.45
	X-ray	0.76	1.24	-0.93	0.57	-0.31
H ₂ HETPP	calculated	1.04	0.62	-1.29	1.05	-1.20
	X-ray	0.95	0.74	-1.17	0.79	-1.08
H ₂ OETPP	calculated	1.20	1.06	-1.34	1.06	-1.34
	X-ray	1.17	1.03	-1.26	1.10	-1.27

^a The values are the average deviation of the two C_b carbons of the corresponding pyrrole ring (quadrant) from the least-squares plane of the four pyrrole nitrogen atoms. Numbering of quadrants is shown in Figure 1. ^b The calculated values were obtained from the semiempirical calculations described in this work, and the X-ray data from ref 3.

following: (1) an increasing long-wavelength (red) shift of all the features in the absorption and fluorescence spectra, (2) a successive increase of the absorption/fluorescence spacing $\Delta(\text{ab/fl})$, (3) diminishing structure in the fluorescence spectra, and (4) progressive shortening of the singlet-excited-state (fluorescence) lifetime. Although the relative structural asymmetries of the molecules may contribute, the finding that these properties follow a trend with ΔC_b suggests that the overall out-of-plane deviation is the overriding factor influencing the photophysical characteristics of nonplanar porphyrins with saddle-type distortions.

It is important to note that above-mentioned photophysical properties of the nonplanar porphyrins studied here are found even in nonpolar solvents such as *n*-hexane and toluene. Thus, the altered static and time-resolved characteristics are intimately associated with the structural/electronic characteristics of the nonplanar porphyrin macrocycle. In other words, properties such as the large absorption/fluorescence spacings and broad fluorescence profiles do not simply reflect the response of the solvent and its interaction with the porphyrin due to photoexcitation (although these factors may contribute), but must substantially involve excited-state structural relaxation of the porphyrin macrocycle. The present results demonstrate that the steric/electronic interactions between nonplanar free base porphyrins and the solvent are stronger than for planar analogues, and are amplified and lead to even more significantly perturbed properties in polar solvents. The increased effects of polar solvents may include (1) specific interactions with pyrrole nitrogens (N–H bonds and lone pairs), which become more accessible to the solvent molecules due to the out-of-plane macrocycle distortion,²² (2) interactions with local dipoles and electronic asymmetries in the distorted porphyrin, and (3) interactions with a permanent dipole moment that the distorted molecule may possess.

It is noteworthy that a macroscopic dipole moment may arise even when a distorted macrocycle is highly symmetric (as is the case for H₂OETPP), and even in the absence of central-metal effects. It is also noteworthy the dipole moment (in addition to local factors) must make a significant contribution to the photophysical properties noted above. This point follows from the fact that a number of the local effects (e.g., accessibility of central nitrogens) derived from distorted macrocycle should also present in saddle-type diacid derivatives of H₂TPP and H₂OEP.⁹ However, the latter molecules possess neither the permanent dipole moment nor the marked dependence of their fluorescence spectra and lifetimes on solvent polarity found for the compounds studied here. Collectively, the local and macroscopic effects of macrocycle distortions afford a wide range of behaviors for the nonplanar porphyrins. These issues are described in more detail in the following.

Characteristics of the Nonplanar Porphyrins in Nonpolar Media. The long-wavelength shifts of the ground-state absorption bands of H₂cTETPP, H₂HETPP, and H₂OETPP are characteristic of the nonplanar porphyrins.^{5–8} Indeed, these shifts track the degree of saddle-type distortion (Figure 2). The red-shifted features can be explained by preferential destabilization of the HOMO's compared to the LUMOs.^{2a,10a,23} The excited-state fluorescence bands are also red shifted from the positions in the planar counterparts (Figure 3). In fact, it is routinely found^{6,7,10} that the emission bands are more red shifted from the planar positions than the absorption features, resulting in unusually large absorption/fluorescence spacings, $\Delta(\text{ab/fl})$. These large spacings can be attributed mainly to the photoinduced changes in porphyrin conformation. Although the large emission

red shifts and $\Delta(\text{ab/fl})$ values are likely dominated by macrocycle distortions, there may be a contribution from macrocycle-nonplanarity-induced rotation of the peripheral *meso*-phenyl rings to more in conjugation with the ring π -system. The dominance of nonplanarity vs phenyl-ring-rotation effects is indicated by calculations,²³ the comparable $\Delta(\text{ab/fl})$ values for H₂OETPP and H₂DPP (dodecaphenylporphyrin),^{7c,e} and the correlation of the $\Delta(\text{ab/fl})$ spectral and ΔC_b distortion parameters.

In general terms, the large absorption/fluorescence spacings are an indicator of greater “conformational flexibility” of the photoexcited nonplanar porphyrins relative to the ground state, and to planar analogues in general. The conformational flexibility of both the ground and the excited states is further illustrated by the increased breadths of the absorption and emission bands and the decreased Soret extinction coefficients relative to nondistorted porphyrins (Table 1). These characteristics can be ascribed in large measure to inhomogeneous broadening due to the presence of multiple accessible conformations in solution. For H₂DPP and other dodecarylporphyrins studied elsewhere, these configurations likely include rotating/tilting of the multiple peripheral aryl rings and their steric/electronic interactions with each other and the macrocycle (which affect nonplanarity).^{7c,e} (These factors no doubt contribute, along with crystal-packing forces, to the finding that many dodecarylporphyrins crystallize in more than one structure, which further demonstrates the energetic accessibility of multiple conformers.⁵) For the molecules H₂cTETPP, H₂HETPP, and H₂OETPP studied here, the relative positions and interactions among the β -ethyl and *meso*-phenyl substituents (and the macrocycle) likely play a similar role in governing the accessible conformations for each chromophore. This view is supported by the increasing optical bandwidths and decreasing vibronic structure (particularly in emission) with the number of β -ethyl groups. Furthermore, the qualitative correlation of these spectral and structural characteristics suggests that increasing the degree of macrocycle distortion is accompanied by an increase in the range of conformers about the mean. Thus, the accessible conformers for each molecule generally represent only modest deviations from the key nonplanar architecture (such as modulation of the pure saddle form for H₂OETPP) rather whole-scale shifts to other nonplanar distortion modes (e.g., ruffling or doming.).

Inhomogeneous spectral effects derived from multiple contributing conformers will be supplemented by homogeneous effects for each conformer. These effects include anharmonic coupling of high frequency in-plane Franck–Condon active vibrations and the low frequency out-of-plane distortion modes, as well as increasing intensity associated with modes not normally vibrationally active as a result of the reduced symmetry in the distorted molecules.^{7c,e} Both effects should contribute to breadths of bands, and especially to the “filling in” of intensity between the normal Q(0,0) and Q(1,0) absorption or Q(0,1) emission bands (Figures 2 and 3). Both the inhomogeneous and the homogeneous spectral effects will be diminished at low temperature. The reasons include (1) lower thermal population of higher vibrational levels of the out-of-plane modes (which have energies^{5b} of only 20–60 cm⁻¹ and thus are populated well above zero point at room temperature), (2) reduced access to conformations requiring the crossing of small barriers, and (3) reduced macrocycle conformational freedom due to the increased rigidity (viscosity) of the microenvironment. Perhaps the most prominent manifestations of these effects are the dependencies of the fluorescence spectra on excitation wave-

length and of the fluorescence-excitation spectra on detection wavelength at cryogenic temperature, where transitions between the individual structures are hindered (Figure 5). The fact that such wavelength-dependent phenomena are not observed at room temperature implies that the barriers between the conformers are relatively small (see also below) and that there are only modest changes in structure between the conformers (as noted above). It must be emphasized again all these consequences of conformational flexibility are manifested for nonplanar *free base* porphyrins, including for the lowest $S_1(\pi,\pi^*)$ excited states of these molecules. Thus, these characteristics are intimately associated with the distorted porphyrin macrocycle and its π -electron system, and do not require effects of a central metal or metal-centered excited states. Furthermore, the identities and range of accessible conformers and associated effects on properties (e.g., optical bandwidths), involve interplay of the macrocycle distortion, peripheral substituents, central nitrogens of the free-base porphyrins (N–H bonds and lone pairs), and both specific and macroscopic interactions with the solvent.

In addition to the static optical properties, two of the most notable photophysical consequences of nonplanar distortion of the porphyrin macrocycle are dramatically reduced $S_1(\pi,\pi^*)$ lifetimes and reduced fluorescence yields. These same perturbations relative to planar H_2 TPP are displayed by nonplanar H_2 -cTETPP, H_2 HETPP, and H_2 OETPP. Furthermore, a number of the observations on these three molecules afford additional insights into the origins of the altered excited-state relaxation properties. It is well documented that the dramatically shortened excited-state lifetimes of the nonplanar porphyrins arise almost exclusively from enhanced nonradiative decay, especially internal conversion to the ground state.^{7,9} The issue now evolving is the underlying physical origin of this effect. The simplest view is that the Franck–Condon factors for radiationless deactivation are enhanced due to increased (horizontal) coordinate displacements and reduced (vertical) energy gaps between the equilibrium positions on the ground- and excited-state potential-energy surfaces. These energy-surface relationships are reflected in the photoinduced conformational change thought to largely underlie the large absorption/fluorescence spacings and in the red shifts of the optical features relative to planar analogues.

This zeroth-order picture assumes that the ground- and excited-state surfaces each have only one accessible minimum, associated with the respective equilibrium configuration. Although correct for normal, planar porphyrins, where there are large, insurmountable barriers for accessing nonplanar conformations, this picture is clearly an oversimplified view of the conformational landscapes of the nonplanar porphyrins.^{7d,e,9} As indicated above, many observations made here and elsewhere indicate that nonplanar porphyrins can access multiple ground- and excited-state conformations. Examples include the large widths of the absorption and fluorescence bands and the large absorption-fluorescence spacings, all of which decrease as the temperature is reduced (Figures 2–4 and Table 1). Likewise, the very short (relative to planar analogues) excited-state lifetimes lengthen as the temperature is lowered (Figure 7, Table 3, and ref 7c). Thus, the ground- and excited-state potential-energy surfaces for the nonplanar porphyrins must have multiple minima separated by small barriers that are surmountable at room temperature. In other words, the “equilibrium form” of each electronic state actually encompasses a number of different configurations (involving the porphyrin macrocycle, its peripheral substituents, and the solvent), each of which contributes to some extent to the static and time-resolved optical properties.

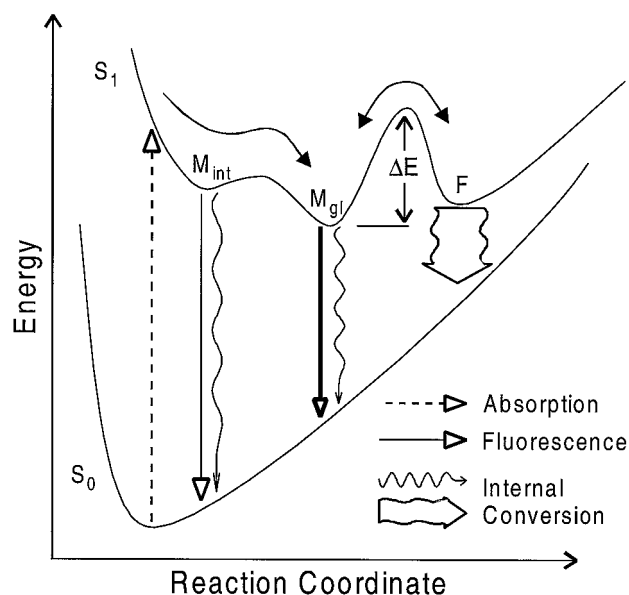


Figure 8. Hypothetical potential energy surface diagram. The thickness of the arrows designate the importance of the fluorescence and internal conversion processes at a particular coordinate relative to each other and to the same processes at other coordinates.

When the temperature is reduced, a smaller subset of *nonplanar* ground- and excited-state conformations more similar to one another dominate the behavior.

We have recently extended this picture to include a new model for the origins of the enhanced nonradiative decay properties of these molecules. This model is illustrated in the simplified schematic diagram given in Figure 8. The key idea is that although the bulk of the emission occurs from conformations at or near $S_1(\pi,\pi^*)$ excited-state minimum (displaced from the S_0 ground-state minimum as in the simple model), the bulk of the nonradiative decay occurs by the traversal of small barriers to other configurations called “funnel points” (F). The funnel geometries have even more enhanced nonradiative decay rates because they have even smaller energy gaps to the ground state and thus even more favorable Franck–Condon factors for internal conversion (as in the energy-gap law for radiationless decay²⁴). At low temperature, it is more difficult to cross the barriers to reach the funnel points. Thus, the fraction of the molecules decaying nonradiatively is decreased, and the excited-state lifetimes (and fluorescence yields) increase toward those of the planar analogues (Figure 7 and Table 3). The lifetimes do not reach those of planar porphyrins because the most populated excited-state configurations, which are nearer the equilibrium form(s), still have enhanced nonradiative decay rates compared to planar analogues (as in the zeroth-order picture given above). As noted above, the various configurations may be associated with a variety of interrelated factors involving the nonplanar distortions of the macrocycle (which may be small deviations from a predominant form), the positions and relative positions of the peripheral substituents (such as the ethyl groups of the compounds studied here), and the disposition and interactions of the solvent molecules with the porphyrin (both specific and macroscopic).

The new model also easily explains the observed shortening of the $^1(\pi,\pi^*)$ lifetimes with an increase of the macrocycle nonplanarity for the three porphyrins studied here. In particular, as the degree of distortion increases, the activation enthalpy (ΔE in Figure 8) progressively decreases from 550 cm^{-1} for H_2 -cTETPP to 430 cm^{-1} for H_2 HETPP and to 220 cm^{-1} for H_2 -OETPP in the nonpolar solvent toluene.²⁵ Similarly, as the

temperature is reduced to 77 K, the static optical properties change toward those of planar porphyrins. It must be emphasized that these changes occur despite the molecules remaining nonplanar, as can be seen, for example, from the fact that the absorption bands are almost as red shifted at low temperature. Rather, fewer conformations are populated (giving reduced bandwidths) and the populated nonplanar excited-state forms have configurations closer to those most populated in the ground state prior to excitation (giving reduced absorption-fluorescence spacings and more emission structure). In fact, as indicated in Figure 8, some of the excited-state configurations receiving preferential population at low temperature may represent secondary excited-state minima that lie along the relaxation pathway from the configurations produced at the instant of (vertical) excitation (intermediate minimum M_{int} in Figure 8). In turn, traversing these secondary configurations and the associated barriers following photoexcitation at room temperature to attain the lower-energy excited-state forms (global minimum M_{gl} in Figure 8) most populated at equilibrium has other implications. For example, the process of visiting such intermediate configurations M_{int} and small barriers helps to explain the "slow" nature of the ~ 10 ps conformational/vibrational relaxation dynamics observed here in the fluorescence time profiles for H_2cTETPP , H_2HETPP , and H_2OETPP and previously in transient absorption measurements on $\text{H}_2\text{-DPP}$.^{7d} In particular, the ~ 10 ps required for this relaxation is slower than the simple vibrational time scale that might have been inferred for a simple downhill relaxation process from the initially excited conformation to the global excited-state minimum M_{gl} (Figure 8). We also note that the two long-lived components of the fluorescence-decay kinetics observed for all three nonplanar porphyrins may result from the coexistence of two statistically populated but unmixed (on the time scale of the excited-state lifetime) excited-state subsystems. Each subsystem would be formed from the same initially excited conformation, and then follow different trajectories (like the one illustrated in Figure 8), each with its own reaction coordinate, activation barriers and funnel points.

Characteristics of the Nonplanar Porphyrins in Polar Solvents. All of the above-mentioned perturbed static and dynamic photophysical properties of these three nonplanar free base porphyrins occur in nonpolar media. Thus, these properties are associated largely with macrocycle nonplanarity and associated electronic perturbations to the porphyrin π -system. Our results also show that the static and time-resolved consequences of nonplanarity are amplified in polar solvents, where the medium's response to macrocycle distortions and more substantial porphyrin-solvent interactions come into play. Again, these solvent interactions may include both local effects (dipoles, electronic asymmetries, accessibility to the central N-H bonds and nitrogen lone pairs) and macroscopic effects that are most easily described in terms of the significant permanent dipole moments that the saddle-shaped free base porphyrins may possess, even if the macrocycle distortions are highly symmetric. In the following, the solvent-polarity dependence of the photophysical properties are discussed mainly in terms of the nonplanarity-induced permanent dipole moments, realizing that the local electronic asymmetries and factors may be significant as well.

An increase in solvent polarity causes H_2cTETPP , H_2HETPP , and H_2OETPP to all have a progressive long-wavelength shift in the ground-state absorption bands, a further loss of the two-banded fluorescence structure, an increase in the absorption-fluorescence spacing, and a decrease in the $S_1(\pi, \pi^*)$ lifetime.

Similar static spectral effects have been found recently for $\text{H}_2\text{-TPP-NO}_2$, in which one β -pyrrole position of planar H_2TPP is substituted with an NO_2 group.²⁶ The presence of a large dipole moment for $\text{H}_2\text{TPP-NO}_2$ (in the porphyrin plane) is expected because of the highly electron-withdrawing character of the single nitro group. The molecules H_2cTETPP , H_2HETPP , and H_2OETPP do not possess pronounced electron withdrawing/donating groups, and the latter molecule is also symmetrically substituted (Figure 1). Nonetheless, for each of these molecules, our semiempirical quantum chemical calculations predict a marked static dipole moment, with a substantial projection orthogonal to the mean nitrogen plane (Figure 1, row E). The origin of these dipole moments can be seen from the following considerations.

It is known that a molecular dipole moment is formed by combination of individual bond dipoles plus the dipole moments associated with the lone pairs residing in the nonbonding hybrid orbitals of any heteroatoms present.²⁷ If the molecule has a center of symmetry, these bond and heteroatom-lone-pair dipole moments sum to zero. A reduction in symmetry due to chemical substitution or structural transformations can result in noncompensation of the individual dipoles to give a net static dipole moment. The existence of nonzero dipole moments in organic molecules generally arises from the C-H bond dipoles, which have values and directions that are strongly dependent on the type of carbon-atom hybridization.²⁷ However, noncancellation of C-H bond dipoles cannot be the source of the permanent dipole moments of the three nonplanar porphyrins studied here. Indeed, in the case of H_2OETPP , all the peripheral H atoms are substituted by ethyl or phenyl groups. Furthermore, our calculations show that replacement of the ethyl groups by H atoms while retaining the same nonplanar structure does not cause a reduction in the value of the molecular dipole moment.

It is clear that the observed static dipole moments of free base porphyrins with saddle-type distortions arise from the nonequivalence of the pyrrole (with N-H bond) and pyrroline (without N-H bond) rings in the porphyrin core. This nonequivalence is a result of the different hybridization of the nitrogen atoms in the pyrrole and pyrroline rings. This situation is the easiest to describe for H_2OETPP , which is symmetrically substituted and adopts a pure saddle conformation (and thus does not have the additional effects of asymmetric substitutions and asymmetric structural distortions operative in H_2cTETPP and H_2HETPP) (Figure 1). Our calculations on $\text{H}_2\text{-OETPP}$ indicate that the two pyrrole nitrogen atoms have positive atomic charge (+0.34) whereas the carbon atoms of these two rings are charged negatively (-0.17 on C_a carbons and -0.096 on C_b carbons). The pyrrole hydrogen atom is charged positively (+0.098). The pyrroline-ring atoms all have negative atomic charge: -0.14 on nitrogen, -0.02 on C_a carbons, and -0.11 on C_b carbons.

The pure saddle conformation of H_2OETPP is such that the Z projections (orthogonal to the mean plane of the four nitrogens) of the dipole moments of two pyrrole rings do not cancel but instead add together. Similar addition of pyrroline dipole moments is observed along Z direction, and the Z projections of the dipole moments of both pyrrole and pyrroline rings have same sign (Figure 1, row D, and Figure 9). Therefore, although all four core nitrogen atoms lie approximately in same plane for a pure saddle structure, the lack of C_4 symmetry and the large tilt of the two pyrrole rings result in a remarkable Z-oriented static dipole moment. Specifically, our calculations indicate that H_2OETPP has a ~ 1.2 D dipole moment that is projected entirely orthogonal to the mean

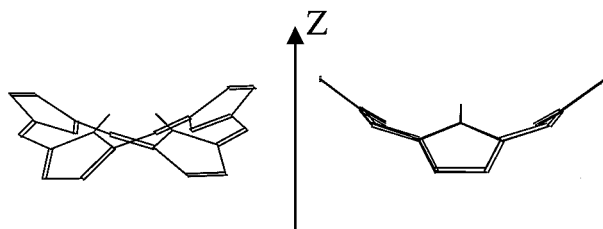


Figure 9. Two side views of H₂OETPP demonstrating structural reasons of a formation of Z-oriented static dipole moment in saddle-shaped free base porphyrins.

nitrogen plane (Figure 1, row E). The dipole moment of H₂-HETPP is even higher (~1.9 D) and makes an angle of ~75° with respect to the macrocycle plane, while the value for H₂-cTETPP is lower (~1.4 D) and the dipole moment is tipped to an ~50° angle. The dipole moments and Z-axis projections of these latter two molecules differ from each other and H₂OETPP due to the asymmetric substitution patterns affecting the charge distributions and the asymmetric structures affecting the cancellation/addition of the contributing dipoles (Figure 1). In contrast, the planar H₂TPP has a negligible static dipole moment.

The static dipole moments found for the nonplanar free base porphyrins investigated here result in additional interactions with the solvent molecules, especially in polar media. The enhanced porphyrin-solvent interactions can be manifest in several ways that add to the spectral characteristics derived directly from macrocycle nonplanarity (as observed in nonpolar solvents). First, the porphyrin-medium interactions can result in additional broadening of the ground-state absorption bands in polar vs nonpolar solvents due to an inhomogeneity of the mutual orientations of dipoles of the porphyrin and solvent molecules. Indeed, such an effect is observed, although it is not large (see Table 1). Second, if the porphyrin dipole moment changes under excitation, subsequent reorientation of polar solvent molecules and energetic stabilization of the excited porphyrin should result in additional long-wavelength shift of the fluorescence spectrum. This contribution to $\Delta(\text{ab/fl})$ is expected to increase with solvent polarity, as is observed (Table 1). Again, it must be noted that the polar solvents may interact with the nonplanar porphyrins not only via a permanent dipole moment (depending on the type of distortion and free base or metal chelate), but also via more specific interactions such as with the central nitrogens (N–H bonds and lone pairs). Additionally, these porphyrin-solvent interactions may in turn further modulate nonplanarity, and electronic asymmetries (including dipole moments) and thus the photophysical behavior relative to the situation in nonpolar media.

This view of motions and interactions of the photoexcited porphyrin and the polar solvent molecules is readily interlaced with the funnel model in Figure 8 to give insights into the shortening of the excited-state lifetimes of H₂cTETPP, H₂-HETPP, and H₂OETPP with increasing solvent polarity (Figure 6 and Table 2).²⁸ In particular, the “distorting” action of the polar solvent on the nonrigid nonplanar porphyrin macrocycle in its excited state may give the system greater access to the funnel geometries (where nonradiative decay is enhanced). Many of the funnel conformations will be more distorted and more polar than those at or near the equilibrium conformation(s) (where most of the fluorescence occurs). Given the complex interplay of steric and electronic porphyrin↔solvent interactions and their effects on solvent reorientations and macrocycle nonplanarity, it is likely that increased excursions to the funnel geometries may occur for more than one reason. One is the lowering of the relevant barriers and a second is an increase in

the effective motions toward the funnel points, both of which should differ depending on the compound and solvent. These interrelated effects may be reflected in the lower activation enthalpy for excited-state decay observed for H₂HETPP in polar vs nonpolar media, and the increased frequency factors for H₂-cTETPP (Table 4). In any event, the solvent and temperature dependencies of the static and dynamic photophysical properties of the nonplanar porphyrins are most readily explained in terms of complex multicoordinate excited-state potential energy surfaces represented in a simple form in Figure 8. These surfaces involve access to multiple configurations (involving strong electronic and steric interplay of the macrocycle, peripheral substituents and solvent) that differ in their energy gaps with the ground state and their radiative and nonradiative decay properties.

Acknowledgment. This research was supported by the U.S. Civilian Research and Development Foundation (Grant No. BC1-105 to V.S.C., V.A.G., and D.H.) and the U.S. National Institutes of Health (Grant No. GM34685 to D.H.). The authors are also grateful to the State Committee for Science and Technology of the Republic of Belarus and INTAS for the financial support (Grant INTAS–Belarus No. 97-0428 to I.V.S., V.A.G., A.H., T.J.S., and V.S.C.).

References and Notes

- (1) (a) Tronrud, D. E.; Schmid, M. F.; Matthews, B. W. *J. Mol. Biol.* **1986**, *188*, 443–454. (b) Martinez, S. E.; Smith, J. L.; Huang, D.; Szczepaniak, A.; Cramer, W. A. In *Research in Photosynthesis*; Murata, N., Ed.; Proceedings of the IXth International Congress on Photosynthesis; Kluwer Academic: Dordrecht, The Netherlands, 1992; Vol. 2, p 495. (c) Ermler, V.; Fritch, G.; Buchanan, S. K.; Michel, H. *Structure* **1994**, *2*, 925. (d) Deisenhofer, J.; Epp, O.; Sinning, I.; Michel, H. *J. Mol. Biol.* **1995**, *246*, 429. (e) Crane, B. R.; Siegel, L. M.; Getzoff, E. D. *Science* **1995**, *270*, 59. (f) Freer, A.; Prince, S.; Sauer, K.; Papaz, M.; Haithornthwaite-Lawless, A.; McDermott, G.; Cogdell, R.; Isaacs, N. W. *Structure* **1996**, *4*, 449. (g) McDermott, G.; Prince, S. M.; Freer, A. A.; Hawthornthwaite-Lawless, A. M.; Papiz, M. Z.; Cogdell, R. J.; Isaacs, N. W. *Structure* **1996**, *4*, 243–251.
- (2) (a) Medforth, C. J.; Senge, M. O.; Smith, K. M.; Sparks, L. D.; Shelnutt, J. A. *J. Am. Chem. Soc.* **1992**, *114*, 9859–9869. (b) Nurco, D. J.; Medforth, C. J.; Forsyth, T. P.; Olmstead, M. M.; Smith, K. M. *J. Am. Chem. Soc.* **1996**, *118*, 10 918. (c) Barkigia, K. M.; Nurco, D. J.; Renner, M. W.; Melamed, D.; Smith, K. M.; Fajer, J. *J. Phys. Chem. B* **1998**, *102*, 322. (d) Senge, M. O.; *Z. Naturforsch* **1999**, *54b*, 821.
- (3) Senge, M. O.; Kalish, W. W. *Inorg. Chem.* **1997**, *36*, 6103.
- (4) (a) Barkigia, K. M.; Berber, M. D.; Fajer, J.; Medforth, C. J.; Renner, M. W.; Smith, K. M. *J. Am. Chem. Soc.* **1990**, *112*, 8851. (b) Barkigia, K. M.; Renner, M. W.; Furenlid, L. R.; Medforth, C. J.; Smith, K. M.; Fajer, J. *J. Am. Chem. Soc.* **1993**, *115*, 3627–3635. (c) Legev, A.; Galili, T.; Medforth, C. J.; Smith, K. M.; Barkigia, K. M.; Fajer, J.; Levanon, H. *J. Phys. Chem.* **1994**, *98*, 2520–2526.
- (5) (a) Sparks, L. D.; Medforth, C. J.; Park, M.-S.; Chamberlian, J. R.; Ondrias, M. R.; Senge, M. O.; Smith, K. M.; Shelnutt, J. A. *J. Am. Chem. Soc.* **1993**, *115*, 581–592. (b) Jentzen, W.; Simpson, M. C.; Hobbs, J. D.; Song, X.; Ema, T.; Nelson, N. Y.; Medforth, C. J.; Smith, K. M.; Veyrat, M.; Maxxanti, M.; Ramasseul, R.; Marchon, J.-C.; Takeuchi, T.; Gaddard, W. A.; Shelnutt, J. A. *J. Am. Chem. Soc.* **1995**, *117*, 11 085–11 097.
- (6) Takeda, J.; Ohya, T.; Sato, M. *Chem. Phys. Lett.* **1991**, *183*, 384–386. (b) Charlesworth, P.; Truscott, T. G.; Kessel, D.; Medforth, C. J.; Smith, K. M. *J. Chem. Soc., Faraday Trans.* **1994**, *90*, 1073–1076. (c) Maiti, N. C.; Ravikanth, M. *J. Chem. Soc., Faraday Trans.* **1996**, *92*, 1095–1100.
- (7) (a) Gentemann, S.; Medforth, C. J.; Forsyth, T. P.; Nurco, D. J.; Smith, K. M.; Fajer, J.; Holten, D. *J. Am. Chem. Soc.* **1994**, *116*, 7363–7368. (b) Gentemann, S.; Medforth, C. J.; Ema, T.; Nelson, N. Y.; Smith, K. M.; Fajer, J.; Holten, D. *Chem. Phys. Lett.* **1995**, *245*, 441–447. (c) Gentemann, S.; Nelson, N. Y.; Jaquinod, L.; Nurco, D. J.; Leung, S. H.; Medforth, C. J.; Smith, K. M.; Fajer, J.; Holten, D. *J. Phys. Chem. B* **1997**, *101*, 1247–1254. (d) Retsek, J. L.; Gentemann, S.; Medforth, C. J.; Smith, K. M.; Chirvony, V. S.; Fajer, J.; Holten, D. *J. Phys. Chem. B* **2000**, *104*, 6690–6693. (e) Retsek, J. L.; Medforth, C. J.; Nurco, D. J.; Gentemann, S.; Chirvony, V. S.; Smith, K. M.; Holten, D. *J. Phys. Chem.*, submitted.
- (8) (a) Drain, C. M.; Kirmaier, C.; Medforth, C. J.; Nurco, D. J.; Smith, K. M.; Holten, D. *J. Phys. Chem.* **1996**, *100*, 11 984–11 993. (b) Drain, C.

M.; Gentemann, S.; Roberts, J. A.; Nelson, N. Y.; Medforth, C. J.; Jia, S.; Simpson, M. C.; Smith, K. M.; Fajer, J.; Shelnut, J. A.; Holten., D. *J. Am. Chem. Soc.* **1998**, *120*, 3781–3791.

(9) Chirvony, V. S.; van Hoek, A.; Galievsky, V. A.; Sazanovich, I. V.; Schaafsma, T. J.; Holten, D. *J. Phys. Chem.* **2000**, *104*, 9909–9917.

(10) (a) Barkigia, K. M.; Chantranupong, L.; Smith, K. M.; Fajer, J. *J. Am. Chem. Soc.* **1988**, *110*, 7566. (b) Shelnut, J. A.; Song, X. Z.; Ma, J.-G.; Jia, S. L.; Jentzen, W.; Medforth, C. J. *Chem. Soc. Rev.* **1998**, *27*, 31.

(11) (a) Franzen, S.; Lambry, B.; Bohn, B.; Poyart, C.; Martin, J.-L. *Nature Struct. Biol.* **1994**, *1*, 230–233. (b) Springer, B. A.; Sligar, S. G.; Olson, J. S.; Phillips, G. N. *Chem. Rev.* **1994**, *94*, 699–714.

(12) Little, R. G.; Anton, J. A.; Loach, P. A.; Ibers, J. A. *J. Heterocycl. Chem.* **1975**, *12*, 343.

(13) Bruggeman, Y. E.; Boogert, A.; Van Hoek, A.; Jones, P. T.; Winter, G.; Schots, A.; Hilhorst, R. *FEBS Lett.* **1996**, *388*, 242.

(14) Van Hoek, A.; Visser, A. J. W. G. *Analytical Instrumentation* **1985**, *14*, 359.

(15) Vos, K.; Van Hoek, A.; Visser, A. J. W. G. *Eur. J. Biochem.* **1987**, *165*, 55.

(16) Stewart, J. J. P. *J. Comput. Chem.* **1991**, *12*, 320.

(17) HyperChem, Molecular Visualization and Simulation, Hypercube, Inc.

(18) (a) Ridley, J.; Zerner, M. C. *Theor. Chim. Acta* **1973**, *32*, 111. (b) Ridley, J.; Zerner, M. C. *Theor. Chim. Acta* **1976**, *42*, 223. (c) Zerner, M. C.; Loew, G. H.; Kirchner, R. F.; Mueller-Westerhoff, U. T. *J. Am. Chem. Soc.* **1980**, *102*, 589.

(19) (a) The microscopic empirical parameter E_T^N (see ref 19b) was used to characterize the solvent polarity. Similar trends are found using the dielectric constant. (b) Reichardt, C. *Solvents and Solvent Effects in Organic Chemistry*; Mir: Moscow, 1991; Chapter 7, pp 524–530.

(20) (a) Analysis shows that the term $A_0 \cdot \exp(-t/\tau_0)$, which contributes to the fluorescence kinetics only on the time scale comparable with the excitation pulse duration, may exhibit both positive and negative signs depending mainly on the fluorescence detection wavelength and the compound studied. We suggest that two different physical processes may contribute to this term. First, the long-wavelength shift of the fluorescence spectrum, which is known to occur for nonplanar porphyrins on the time scale of ~ 10 ps,^{7d} should result in negative sign of A_0 at the detection wavelengths near maximum of the static fluorescence spectrum. Second, an ultrafast (time scale of about 1 ps) transformation of the “hot”

fluorescence, which has been recently detected for different planar (meso-substituted) porphyrins on the short-wavelength side of the static fluorescence spectrum,^{20b,20c} to the “cooled” fluorescence may result in either a positive or negative sign of A_0 , depending on the fluorescence detection wavelength. In general, the relative contributions of these two effects, and thus the sign of the associated term in the fluorescence time profile (A_0), will depend on the detection wavelength and the time-response and overall time scale of the measurements. (b) Akimoto, S.; Yamazaki, T.; Yamazaki, I.; Osuka, A. *Chem. Phys. Lett.* **1999**, *309*, 177. (c) Galievsky, V. A.; Dobkowski, J.; Waluk, J.; Chirvony, V. S., to be published.

(21) Ethyl groups are mildly electron donating in character while phenyl groups substituents are weakly electron withdrawing.

(22) (a) Takeda, J.; Sato, M. *Chem. Lett.* **1995**, 971. (b) Li, M.; Xiao, Z.; Xiong, H.; Lu, Z. *Spectrochim. Acta, Part A*, **1997**, *53*, 1691.

(23) Parusel, A. B. J.; Wondimagegn, T.; Gosh, A. *J. Am. Chem. Soc.* **2000**, *122*, 6371.

(24) Siebrand, W. J. *J. Chem. Phys.* **1967**, *46*, 440–447.

(25) The frequency factor in the Arrhenius expression for the dependence of the $S_1(\pi, \pi^*)$ -state deactivation rate on temperature is found to be not strongly dependent on the macrocycle nonplanarity in nonpolar solvents, and lies (in toluene) in the range of 5×10^9 s⁻¹ for H₂cTETPP and H₂-HETPP and even slightly decreases for H₂OETPP (3×10^9 s⁻¹). However, in polar solvents such as acetonitrile, the frequency factor is much more sensitive to the porphyrin nonplanarity and asymmetry and changes from 37×10^9 s⁻¹ for H₂cTETPP to 6×10^9 s⁻¹ for H₂HETPP and 8×10^9 s⁻¹ for H₂OETPP.

(26) Chirvony, V. S.; van Hoek, A.; Schaafsma, T. J.; Pershukovich, P. P.; Filatov, I. V.; Avilov, I. V.; Shishporenok, I. V.; Terekhov, S. N.; Malinovskii, V. L. *J. Phys. Chem. B* **1998**, *102*, 9714.

(27) Minkin, V. I.; Osipov, O. A.; Zhdanov, Yu. A. *Dipol'nyie Momenty (Dipole moments)*; Khimiia: Leningrad, 1968; Chapter 3 (in Russian).

(28) We note that the standard explanation of a drop in energy and contribution of charge-transfer states to nonradiative decay does not play a significant role (if any) in these free-base porphyrins. In particular, the only possible charge-transfer states involve the macrocycle and the peripheral meso-phenyl rings, and our calculations suggest that these states are not sufficiently low in energy for our compounds as well as for the related planar porphyrins. Such additional states did not appear also in case of a rotation of the phenyl substituents toward their coplanarity with the “porphyrin plane”.